Water Air Soil Pollut (2023) 234:286
https://doi.org/10.1007/s11270-023-06245-4

Application of High-Resolution Near-Infrared Imaging Spectroscopy to Detect Microplastic Particles in Different Environmental Compartments

Matthias Munz · Jasper Kreiß · Lisa Krüger · Lena Katharina Schmidt · Mathias Bochow · Marius Bednarz · Claus Gerhard Bannick · Sascha E. Oswald

Received: 14 September 2022 / Accepted: 18 March 2023 / Published online: 18 April 2023

Abstract Microplastic particles (MPP) occur in various environmental compartments all over the world. They have been frequently investigated in oceans, freshwaters, and sediments, but studying their distribution in space and time is somewhat limited by the time-consuming nature of the available accurate detection strategies. Here, we present an enhanced application of lab-based near-infrared imaging (NIR) spectroscopy to identify the total number of MPP, classify polymer types, and determine particle sizes while maintaining short measuring times. By adding a microscopic lens to the hyperspectral camera and a cross slide table to the setup, the overall detectable particle size has been decreased to 100 µm in diameter. To verify and highlight the capabilities of this enhanced, semi-automated detection strategy, it was applied to key areas of microplastic research, such as a lowland river, the adjacent groundwater wells, and marine beach sediments. Results showed mean microplastic concentrations of 0.65 MPP/L in the Havel River close to Berlin and 0.004 MPP/L in the adjacent groundwater. The majority of MPP detected in the river were PP and PE. In 8 out of 15 groundwater samples, no MPP was found. Considering only the samples with quantifiable MPP, then on average 0.01 MPP/L was present in the groundwater (98.5% removal during bank filtration). The most abundant polymers in groundwater were PE, followed by PVC, PET, and PS. Mean MPP concentrations at two beaches on the German Baltic Sea coast were 5.5~MPP/kg at the natural reserve Heiligensee and Hüttelmoor and 47.5 MPP/kg at the highly frequented Warnemünde beach.

Keywords Microplastic particles · Surface water · Groundwater · Bank filtration · Beach sediments · Baltic Sea · NIR spectroscopy

Supplementary Information The online version contains supplementary material available at https://doi.org/10.1007/s11270-023-06245-4.

M. Munz (✉) · J. Kreiß · L. Krüger · L. K. Schmidt · S. E. Oswald
Institute of Environmental Science and Geography, University of Potsdam, Karl-Liebknecht-Str. 24-25, 14476 Potsdam, Germany
e-mail: munz@uni-potsdam.de

M. Bochow
Remote Sensing and Geoinformatics Section, GFZ German Research Centre for Geosciences, Telegrafenberg, 14473 Potsdam, Germany

M. Bednarz · C. G. Bannick
German Environment Agency (UBA), Corrensplatz 1, 14195 Berlin, Germany

1 Introduction

Microplastic particles (MPP) are found ubiquitously in the environment. While research on marine MPP abundances began decades ago, the focus of current research activities has shifted towards freshwater resources as well as aquatic sediments and terrestrial

soils. Several scoping reviews emphasise the occurrence of microplastics in rivers (Eerkes-Medrano et al., 2015; Kumar et al., 2021; Li et al., 2018). Detected riverine microplastic concentrations range from a few MPP/m^3 to around 10,000 MPP/m^3 close to the water surface in an urban watercourse (Kumar et al., 2021; Schmidt et al., 2018).

Depending on their physical properties, MPP may be transported along a river over long distances or infiltrate and accumulate in riverbed sediments (Boos et al., 2021; Nizzetto et al., 2016), where a wide range of plastic polymers with total concentrations of around 1000 MPP/kg dry weight of sediment and sizes up to 5000 µm have been found (Frei et al., 2019). Fine particles can even be mobile in streambed sediments (Drummond et al., 2020) and alluvial aquifers (Goeppert & Goldscheider, 2021; Viaroli et al., 2022). Concordantly, particles > 100 µm were found to be mobile in laboratory experiments, where particle mobility strongly depended on relative pore and particle sizes (Waldschläger & Schüttrumpf, 2020). At the other end, MPP of up to 150 µm and even 374 µm in size were detected in drinking water production wells and tap water, with concentrations of up to 7 MPP/m^3 (Mintenig et al., 2019) and 74 MPP/m^3 (Kirstein et al., 2021; Pittroff et al., 2021), respectively. Only few studies exist that assess microplastic contamination of groundwater resources (Johnson et al., 2020; Panno et al., 2019; Samandra et al., 2022) with little focus on the potential risk of MPP leaching into groundwater by bank filtration (Johnson et al., 2020). Here, particle transport may be facilitated by high flow velocities through medium- to coarse-grained sand, comparable to pronounced hyporheic exchange fluxes through distinct geomorphological riverbed structures (Frei et al., 2019; Munz et al., 2017).

With respect to marine MPP, more knowledge exists on microplastic pollution and accumulation in beach sediments (Harris, 2020; Hidalgo-Ruz et al., 2012). In the Baltic Sea, for example, microplastic concentrations span several orders of magnitude, from less than ten MPP/kg beach sediments at German coasts (Dekiff et al., 2014; Stolte et al., 2015), via tens of MPP/kg at German (Esiukova et al., 2021; Schröder et al., 2021), Polish (Graca et al., 2017) and Russian coasts (Esiukova, 2017) to hundreds of MPP/kg at German (Stolte et al., 2015) and Polish (Urban-Malinga et al., 2020) coasts. Besides this large-scale variability, only a few studies have focused on the small-scale variability in MPP abundances along beach transects or within sample plots.

Analyzing spatial patterns in MPP abundances requires large numbers of environmental samples. While water sampling is usually done with filters and sieves, sediment samples are treated by density separation to extract MPP for spectroscopic analyses (Braun et al., 2021; Hidalgo-Ruz et al., 2012; Wang & Wang, 2018). Preferably, polymer identification should be done via an automatic analysis of their chemical composition to assure a reliable and user-independent assessment of MPP (Löder & Gerdts, 2015). The most frequently used methods are Fourier transform infrared (FT-IR) spectroscopy, Raman spectroscopy, and pyrolysis–gas chromatography-mass spectrometry (GC/MS) (Braun et al., 2021; Koelmans et al., 2019; Li et al., 2018). Tomography methods represent an alternative for investigating the presence and fate of microplastics in the environment, but so far they have been applied only rarely (Barroso et al., 2019; Sagawa et al., 2018; Tötzke et al., 2021). In summary, the available analysis tools complement each other, but none can be considered the gold standard for analysing all particle types and matrices (Primpke et al., 2020a).

Recently, near-infrared (NIR) imaging spectroscopy has been used for microplastic analyses in a growing number of studies (Faltynkova et al., 2021; Ivleva, 2021; Weisser et al., 2022). Within the last decade, we have developed -in cooperation with other researchers from different projects- and applied NIR imaging spectroscopy with semi-automated MPP identification to detect the presence of MPP in aquatic environments (Atwood et al., 2019; Piehl et al., 2020; Schmidt et al., 2018) (please note that these publications use the term ‘short-wave infrared’ (SWIR) instead of NIR to refer to the wavelength range 1400–3000 nm, which is common in the remote sensing community). In these previous freshwater studies, NIR imaging spectroscopy provided a reliable method to determine polymer types of particles as small as 450 µm. In particular, it allowed MPP detection for a large number of environmental samples in a short time compared to other methods. Further improvements of NIR imaging spectroscopy generally encountered are the increase in spatial resolution to detect smaller MPPs and the development of more robust models for data analysis (Faltynkova et al., 2021).

By adding a microscopic lens to the hyperspectral camera and a cross slide table to the setup, the overall detectable particle size has been decreased to 100 µm in diameter. This expands the application of the near- infrared imaging spectroscopy also to groundwater samples in which the transport of MPP is restricted by the porosity of the aquifer material and it is assumed that only smaller fractions of MPP particles occur.

In this study, we present methodological refinements of our NIR imaging spectroscopy approach and expand the application to samples of groundwater and beach sediments in addition to a river, so that the method is exemplarily applied to key areas of microplastic research. We analysed a total of 82 environmental samples in order to (i) quantify the MPP load of a lowland river, (ii) assess the potential risk of MPP leaching into the groundwater during bank filtration, and (iii) capture the spatial heterogeneity of MPP in beach sediments.

2 Methods

In the following, we describe the study area and sampling strategy of each sample type, namely surface water (Section 2.1.1), groundwater (Section 2.1.2), and beach sediments (Sections 2.2.1 and 2.2.2), including the type-specific laboratory treatments. In Section 2.3, we present the details of the polymer identification with NIR imaging spectroscopy, which was applied to all sample types.

To avoid contamination, plastic-free clothing and instruments were used whenever possible, and all working surfaces and materials were cleaned with a 30% ethanol solution made from distilled and filtered water and filtered ethanol (CA filter with a pore size of 0.45 µm). Furthermore, we took samples of the presumably less contaminated groundwater before sampling the river, to minimize the risk of cross-contamination. Between any two samples, we carefully rinsed all materials (e.g. plankton net, sieves) to avoid cross contamination. In order to identify and evaluate possible sources of contamination in this study, all processing and evaluation steps were also carried out on blind samples (Section 2.4).

2.1 Freshwater Samples

2.1.1 Surface Water Samples

We chose a canal of the Lower Havel federal waterway downstream of the City of Berlin for sampling, due to its proximity to the groundwater wells (Section 2.1.2). Three sets of samples were collected at monthly intervals from May to July 2016, at five locations in a 200 m transect along the canal in approximately equidistant intervals of 40 m (Fig. 1a). Roughly, the topmost 5 cm of the water body were sampled with a glass bailer at three (1^{st} sampling campaign) to five (2^{nd} and 3^{rd} campaigns) points by drawing 20 L (1^{st} and 2^{nd} campaigns) and 60 L (3^{rd} campaign), following the procedure of Schmidt et al. (2018). The collected water was then poured through a plankton net (20 µm mesh size) and its volume was measured with a bucket placed underneath the plankton net. The particles that remained in the net were flushed into 1 L glass bottles with filtered ambient water.

2.1.2 Groundwater Samples

Five groundwater (GW) wells at a bank filtration site adjacent to the canal were sampled on the same day as the river. The wells are located approximately 15 m inland from the surface water (SFW) observation points (Fig. 1a). At GW1 and GW5, two observation wells each were placed together with different filter screen elevations, with the upper and lower ones located approximately 24 m a.s.l. and 18 m a.s.l., respectively. The portion of SFW in the aquifer at the GW wells is above 94%. Subsurface residence times in the sandy to gravely aquifer range from 18 days at $GW1_{upper}$ to 59 days at $GW5_{upper}$ (Munz et al., 2019).

To take groundwater samples, we positioned an Eijkelkamp MP1 pump with a connected Teflon hose in the well several meters below the water level but clearly above the ground of the well. Pumping rates varied between 12 and 20 L/min depending on the exact sampling depth and groundwater temperature. A minimum of 1.5 times the well volume was discarded before sampling. After the temperature, oxygen content, redox potential, and pH-value of each well stabilized, the pumped water was assumed to be representative of the groundwater and the sampling began. For each sample, 200 L

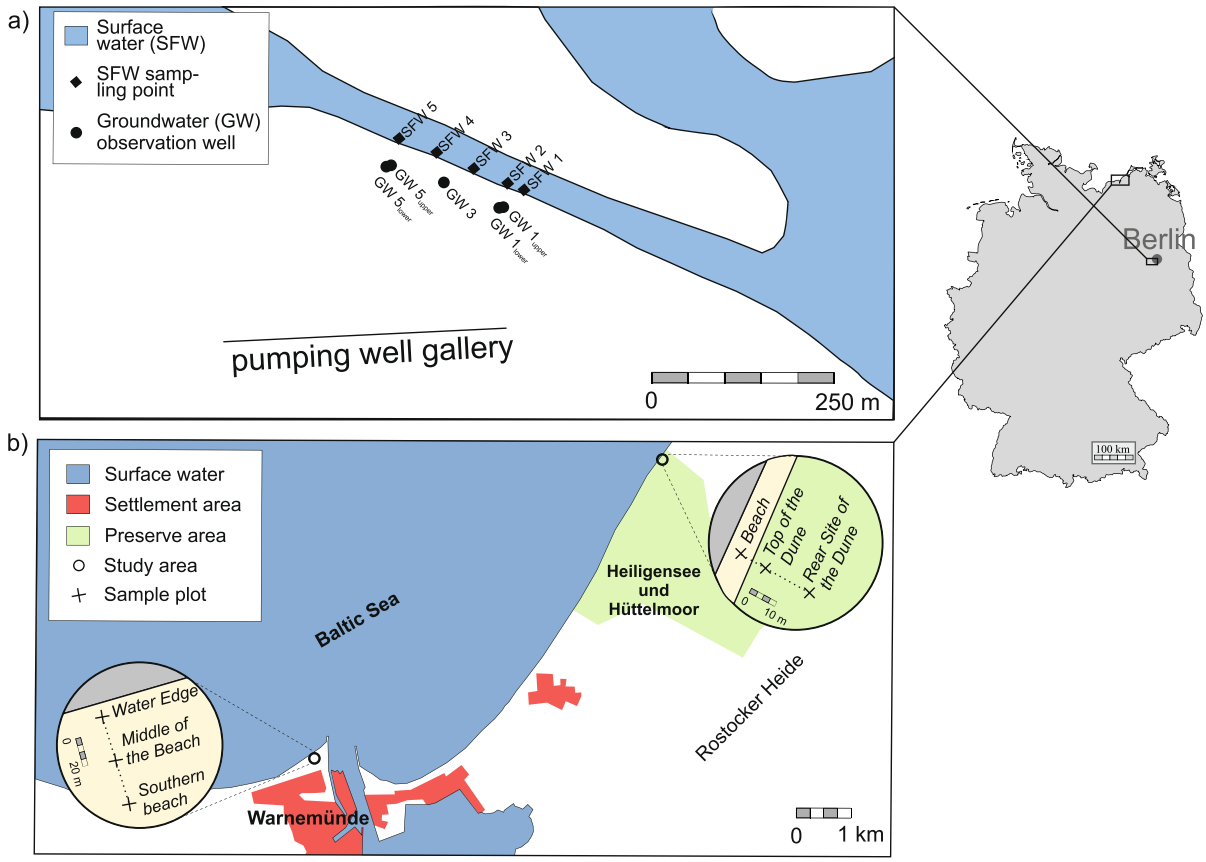

Fig. 1 Plan view of the freshwater (**a**) and sediment sampling sites (**b**)

(1st and 2nd campaigns) and 600 L (3rd campaign) of groundwater were strained through a plankton net with a mesh size of 20 µm. Once the desired volume was reached, the remains in the plankton net were flushed into 1 L glass bottles with filtered ambient water.

All freshwater and groundwater samples were poured through a 20 µm stainless steel analytical sieve in the laboratory. The remaining particles were transferred into glass beakers, covered with lids made of tin foil and dried in a drying cabinet at 70 °C for at least 24 h. Subsequently, 80 ml of 30% H_2O_2 was added to each sample to reduce organic material. The samples were stirred with a magnetic stirrer with glass-coated stir bars for at least 24 h and then left in the H_2O_2 for a week inside a fume cupboard. Afterwards, each sample was rinsed with filtered water in a 20 µm sieve to remove the hydrogen peroxide.

2.2 Sediment Samples

A total of 54 beach sediment samples were taken along transects from two stretches of beach along the Baltic Sea coast near Rostock, Germany. Specifically, we selected a natural reserve area and a touristic beach in order to test the density separation method on a presumably broad range of plastic polymers in beach sediments and to emphasize spatial patterns in the microplastic pollution.

2.2.1 Beach Transect Heiligensee and Hüttelmoor

The beachfront of the 540 ha natural reserve Heiligensee and Hüttelmoor (Fig. 1b), located between Rostock and Graal-Müritz, has been a research site for fluid dynamics studies over the last years (Jurasinski et al., 2018; Miegel et al., 2017; Schreiber et al., 2021). This part of the beach is only occasionally

frequented by hikers and walkers. The samples were taken in December 2019 from a 35 m long transect that was placed perpendicular to the coastline. Nine samples each were taken on the beach, on top of the dune, and at the rear site of the dune (Fig. 1b).

2.2.2 Beach Transect Warnemünde

Warnemünde beach, located in the northern district of Rostock, is strongly influenced by human activities. At the start of every new summer season, almost 15,000 cubic meters of sand that the wind has blown onto the dunes and into the sand traps during winter are brought back to the beach and distributed by heavy machinery. Sediment samples at the beach were taken in March 2020 perpendicular to the coast in a transect of approx. 70 m in length (Fig. 1b). As for the natural reserve, samples were taken at three locations: At the water's edge located in the North, in the middle of the beach, and at the southern part of the beach, with nine samples each.

2.2.3 Sampling Strategy

The beach surface at each location along the transects Heiligensee and Hüttelmoor and Warnemünde was cleaned of major contamination or disruptive objects (such as plastic bag parts, cigarette butts, bottle caps) and any vegetation was carefully removed. A sample pit was then dug at each location, measuring approx. 70 × 80 × 60 cm (L × W × D) and reinforced on the sides with wooden planks. Samples were taken from a straight profile wall with a 100 cm^3 stainless steel cylinder, which had a length of 40.5 mm and an inner diameter of 57 mm. Three samples each were taken at 5 cm, 20 cm, and 40 cm below the beach surface. A distance of 15 cm was maintained between the samples of a layer. The sediments were stored and transported in aluminum dishes or laboratory glass bottles.

The sediment samples were dried at 60 °C for 48 h and subsequently sieved through a stainless steel sieve with a 20 cm diameter and a mesh size of 2 mm (Retsch GmbH, Germany). Larger soil agglomerates were crushed and clearly recognizable plastic particles that got stuck in the sieve were transferred using tweezers. The sediment fraction > 2 mm was optically analyzed. In order to separate microplastic particles from the denser matrix components < 2 mm, we used a sodium iodide solution with a density of approx. $1.8 \frac{g}{cm^3}$ to separate even highly dense pristine polymer materials such as PVC or POM (Dekiff et al., 2014; Quinn et al., 2017). The samples were placed into 250 ml wide-neck Erlenmeyer flasks, which were then filled up to about half with the density solution. The mixture was then stirred for 2 min with a stainless steel spatula (I) and treated for 2 min in an ultrasonic bath (II) to destroy soil agglomerates (steps I and II were repeated once more). Afterwards, the Erlenmeyer flasks were filled to the neck with the density solution and left for 24 h. Subsequently, all floating compounds were captured by direct vacuum filtration (Vacuubrand Vario Select), poured through a filtration funnel with a 6 µm stainless steel mesh (Sartorius, Germany), and transferred with an ethanol solution into pre-cleaned transportation glass jars (Bednarz et al., 2020).

2.3 Semi-automated Identification of MPP

2.3.1 Preparation of Glass Fibre Filters

Prior to imaging, the samples were filtrated from the glass transportation jars onto binder-free glass fibre filters (Macherey–Nagel MN 85/90 BF, 47 mm) using a hand-operated glass filtration device (Sartorius) to guarantee a homogenous distribution of the particles on the filter surface. The filters were then placed in lockable plastic Petri dishes (Millipore SAS, sterilized 47 mm) for the first two SFW sampling campaigns and on glass petri dishes using metal tweezers for all other samples (third SFW sampling campaign and beach samples) and dried at 50 °C for 24 h. To prevent the filters from sticking to the bottom of the glass after drying, a small, folded piece of aluminium foil was placed under each filter.

2.3.2 Near-Infrared Imaging Spectroscopy with HySpex

We used a hyperspectral HySpex SWIR-320 m-e camera (Norsk Elektro Optik AS (NEO)) to record the light reflected by the filters in the near-infrared range (968 to 2498 nm wavelength, recorded by 256 channels with a band width of 6 nm). A row of five filters was placed on a translation stage and moved through the sensor's field of view. The HySpex sensor is a line scanner that records a scene line by line, with each line consisting of 320 pixels. For this

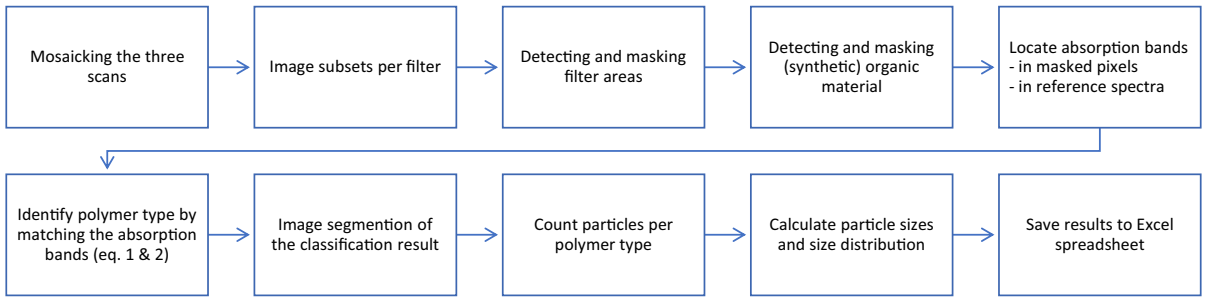

Fig. 2 Flow chart showing the basic steps of PlaMAPP to identify polymer types and determine particle sizes

purpose, the speed of the translation stage is synchronized with the recording speed of the HySpex sensor. To achieve a finer resolution of the recorded pixels, a microscopic lens was attached to the sensor, which decreased the pixel size from the previous 280 µm (as used in Schmidt et al., 2018) to 50 µm. As the linear field of view was reduced to 16 mm due to the microscopic lens, the filters with a width of 47 mm had to be scanned in three strips with 2–3 mm overlap in order to support accurate mosaicking of the three image strips. This was realized by moving the row of 5 filters with a cross slide table between the three scans. As a known spectral reference, a 95% white reference (Zenith Lite ® 90% or 95% by SphereOptics) was placed at the beginning of each scan to convert the measured image spectra into reflectance units afterwards. The spectral measurement of each image pixel was averaged from eight single measurements in order to acquire a high signal-to-noise ratio.

2.3.3 *Data Processing and Identification of Microplastic Particles*

The identification of MPP is mainly based on the calculation of spectral distances between absorption bands of the recorded pixel and reference spectra ($penalty\_score_j$). Therefore, the recorded spectra of the three image stripes were corrected for bad and dead pixels, converted into reflectance units using the absolute reflectance spectrum of the calibrated white reference and merged into one image (mosaicking) (Scheffler, 2021; Scheffler et al., 2017). To identify the polymer types, we applied the PlaMAPP (Plastic Mapper) algorithm developed by Mathias Bochow and initially described in Schmidt et al. (2018). Firstly, image sub-setting is conducted to generate a subset per filter and the filter areas are masked (Fig. 2). Afterwards, only pixels with organic or synthetic polymer materials are selected. This can be achieved by applying a threshold to the absorption intensity between 1550 and 1850 nm wavelengths, as all types of plastic polymers show strong absorption within this spectral region (first overtone absorption band of CH-, CH2-, and CH3-bonds). The threshold was chosen empirically according to the noise level of the data. The spectra of the masked pixels are then converted into the continuum removed form by implementing an adapted algorithm developed by Mielke et al. (2015) into PlaMAPP.

The assignment of an image pixel (measured spectrum) to a polymer type is based on $penalty\_score_j$ [nm] calculated for each reference spectrum j within the PlaMAPP reference library ($j = 1 \ldots m$). Key here is the comparison of the wavelength of a particular absorption band a_pix_k [nm] in the pixel spectrum (k being the index of all absorption bands observed; $k = 1 \ldots n\_pix$) with all possible matching absorption bands in all reference spectra (l being the index of all absorption bands in the reference spectrum j; $l = 1 \ldots n\_ref_j$). For that, firstly, the number of matches $n\_Matches_j$) of absorption bands in the pixel spectrum compared to all absorption bands in the reference spectrum j is identified, allowing for a given small tolerance (Tol [nm]) to be counted as a match.

$$n\_Matches_j = \sum_{k=1}^{n\_pix} \sum_{l=1}^{n\_ref_j} \begin{cases} 1; & if\ a\_ref_{j,l} - Tol \le a\_pix_k \le a\_ref_{j,l} + Tol \\ 0; & else \end{cases} \qquad (0 \le n\_Matches_j \le n\_pix) \tag{1}$$

Absorption bands that occur between 1370 and 1470 nm or 1910 and 1950 nm are excluded, because in these two regions the absorption is dominated by the presence of water, which is a typical indication of organic matter.

Then, we define the fraction of how many of the absorption bands are matching, accounting for the fact that the number of absorption bands may be different in the pixel spectrum compared to the reference spectrum *j*.

$$match\_fract_j = \frac{n\_Matches_j}{{}^1/_2 \bullet \left(n\_pix + n\_ref_j\right)} \quad (0 \le match\_fract_j \le 1) \tag{2}$$

Furthermore, we evaluate how much the matching absorption bands are shifted in wavelength, by calculating an average square mean root shift of absorption bands based on the ones found in the pixel spectrum (after resorting a_pix_i and $a\_ref_{j,i}$ to have indexed all matching ones first and in the same order, running up to $n\_Matches_j$). The square mean root measure was chosen instead of the far more common root mean square measure because we want the small differences to be weighted stronger than the large differences, since all polymers have absorption bands in the same spectral regions and therefore small shifts in band position indicate a different polymer.

$$shift\_average_j = \frac{\left(\sum_{j=1}^{n\_Matches_j} \sqrt{\left|a\_ref_{j,i} - a\_pix_j\right|}\right)^2}{n\_Matches_j} \quad [\text{nm}] \tag{3}$$

The $penalty\_score_j$ for a certain reference spectrum *j* is subsequently calculated as a combination of the average square mean root shift and the fraction of matched absorption bands, but only if there is a minimal number of three matching pairs of absorption bands:

$$penalty\_score_j = \begin{cases} NaN; & if\ n\_Matches_j < 3 \quad (4a) \\ \frac{shift\_average_j}{match\_fract_j^2}; & else\ if\ any\ \left|a\_ref_{j,i} - a\_pix_i\right| > \Delta\lambda\ for\ i = 1 \ldots n\_Matches_j \quad (4b) \\ scaleConst \times \left(\frac{1 - match\_fract_j^2}{match\_fract_j^2}\right); & else \quad (4c) \end{cases}$$

where Δλ is the spectral resolution of the recorded spectrum and *scaleConst* is an arbitrary penalty level that is used only if all matches are within Δλ, i.e. fall in the same spectral channel, implying that $shift\_average_j$ is zero. In our study, *scaleConst* was set to 9.6 nm and *Tol* was set empirically to 2 nm in order to define a stringent threshold criterion to reduce the number of false positive classifications in the final results. As the actual HySpex spectral resolution was Δλ = 6 nm, this implied that only the absorption bands recorded in the same spectral channel are counted as a match according to Eq. (1) and thus Eq. (4b) is not used but instead Eq. (4c), if $n\_Matches_j$ is larger than or equal to 3. Thus, some of the parameters in Eqs. (1) to (4) were set empirically but there are no remaining free parameters in the formulas that need to be optimized. In the current study, the reference spectrum *j* with the largest match fraction will be assigned the lowest $penalty\_score_j$.

Finally, each image pixel is assigned to the polymer type with the lowest penalty score if this penalty score lies below or equal to a threshold of 2 nm; otherwise, it is classed as "unknown organic" to avoid false positive classifications based on too few matches among the ones possible. In the current study, a reference spectrum *j* has to have at least a $match\_fract_j$ of 0.9 to be assigned as a polymer type to the pixel.

Afterwards, all adjacent pixels (8-connectivity) of the same polymer type are grouped into one microplastic particle (image segmentation), and the latter are then subsequently numbered and counted per polymer type. If a polymer type is assigned to a single isolated pixel, it is excluded from the microplastic detection results, since the accuracy of the classification increases significantly with the number of neighbouring pixels that are assigned to the same polymer. Consequently, the minimum detectable MPP size is about 100 µm in diameter (two neighbouring pixels assigned to the same polymer type). As fibers are typically much thinner than one pixel, they are generally not detected by PlaMAPP, which is a limitation of the approach presented.

At the time of processing, the algorithm was capable of classifying polyethylene (PE), polypropylene (PP), styrene polymers (PS) (as a group consisting of polystyrene, acrylonitrile–butadiene–styrene and

styrene-acrylonitrile), polyvinyl chloride (PVC), Polyethylene terephthalate (PET), ethylene–vinyl acetate (EVAC) and ethylene vinyl alcohol (EVAL) (as a group), polyamide (PA), polycarbonate (PC), polyurethane (PU), polyoxymethylene (POM), and polymethyl methacrylate (PMMA).

2.3.4 Visual Validation

For the final declaration, we visually compared the polymers determined by the algorithm with reference spectra of a spectral library using the software *ENVI*. The identified MPP were counted and marked, and their particle sizes (the maximum diameter, the minimum diameter, and the number of pixels) were manually determined. To prevent false-positive classifications, we visually checked and corrected PlaMAPP's classification results based on previous experiences with common misclassifications. PlaMAPP-detected particles were rejected if they did not show typical plastic-like characteristics (such as sharp breaking edges, unnatural colors, foamy textures, or plain surfaces) or if they showed characteristic features of organic material (such as cell textures, leaf veins, or insect body parts).

To validate the performance of the applied MPP classification scheme, the entire filter area was additionally searched under the microscope for potential particles incorrectly rejected by the algorithm (false negatives).

2.4 Blind Samples

In total, 22 blind samples were processed alongside the water samples. Of these, one blind sample was initiated in the field: the plankton net was exposed to atmospheric conditions, rinsed with filtered and ambient water and poured into pre-cleaned glass bottles. The other 21 blind samples were started in the laboratory and sieved, put in the drying oven, stirred for 24 h with hydrogen peroxide, and filtered onto glass fibre filters. Possible contamination sources like abrasion particles from the well casing (blue PVC), the plastic Petri dish used during the first two freshwater sampling campaigns (transparent PS), and the rubber seal used with the glass bottles and transportation jars were excluded from the results of the actual sample filters.

Five blind samples were processed alongside the beach sediment samples. The transportation jars were opened and placed beside a sampling pit to be exposed to potential atmospheric contamination for a total of three minutes. These blind samples were treated the same way as the sediment samples; they were in the drying oven, treated with sodium iodide, put through the filtration system, and filtered onto glass fibre filters. Only one unspecified microplastic particle was identified in all blind samples, giving evidence of minimal sample contamination.

Statistical data analyses were performed based on the corrected counts using the software R (R Core Team, 2021). Normality tests were done by a Shapiro test. In order to identify spatial and temporal differences in MPP occurrence, we calculated the ANOVA test statistic. A significance level of $\alpha = 0.05$ was taken as a basis for all statistical tests.

3 Results and Discussions

3.1 Critical Reflection on MPP Detection and Analysis Using NIR Imaging and PlaMAPP

We identified and analyzed MPP by applying NIR imaging spectroscopy with a semi-automated analysis approach (PlaMAPP classification algorithm followed by visual inspection). Our results highlight that NIR is an accurate and non-destructive approach to identify MPP consisting of various polymer types and sizes. Compared to previous studies (e.g. Schmidt et al., 2018), we significantly reduced the MPP size detection limit from 450 to 100 µm. This is a significant improvement, especially as it facilitates the detection of MPP in size classes relevant to transport within pores of soils and sediments (see, e.g., Frei et al., 2019, Mintenig, et al. 2019; Kirstein et al., 2021, and also Section 3.2.2). As a consequence of using the microscopic lens, we had to record the filters in three slightly overlapping strips (see Section 2.3.2). Initial concerns that particles might be overlooked or counted twice due to imprecise mosaicking were addressed by an extensive visual validation (Section 2.3.4) that did not reveal any particles that had been missed or counted twice due to mosaicking artefacts. Similarly, the number of particles not recognized by PlaMAPP, i.e. the false negatives identified through the visual validation of the entire filter,

was small. In the freshwater samples, only 24 particles showing typical plastic-like characteristics were additionally found, whereas only two false-negative particles were found in the beach sediment samples. These particles clearly showed properties of plastic polymers but were not assigned to a particular type of plastic by the PlaMAPP algorithm. Suggested reasons for this are (i) missing references of the specific polymer type in the reference library, (ii) physical or chemical alterations of known polymers during transport or (iii) the quite stringent tolerance of 2 nm to calculate the *penalty_score*. However, the low number of false negatives with respect to the total number of classified particles by PlaMAPP highlights the high sensitivity of the PlaMAPP classification results.

Nevertheless, several types of misclassifications occurred in the PlaMAPP results themselves (false positives) and needed to be corrected manually. Mainly, misclassifications occurred if non-plastic objects showed absorption patterns that are very similar to those of plastic materials. In particular, organic objects in the sediments were sometimes wrongly classified as PE particles, and various chitinous exoskeletons in the groundwater samples were misclassified as PA for this reason. Fortunately, these misclassifications are known from previous studies and can be identified and corrected by examining their spectra in ENVI. However, this misclassification can substantially be reduced by continuously including individually measured NIR spectra of site-specific organic objects in the PlaMAPP reference library, which would finally cause higher penalty scores between the unknown particle and the organic object versus PE/PA.

A new issue that frequently occurred with the microscopic lens, but not with the 30 cm lens, were misclassifications of single pixels due to interference fringes in the spectra. These caused numerous random absorption features that could coincide with those of the plastic polymers from the library. This phenomenon, albeit well known (Jeszenszky et al., 2004), is unfortunately not easy to correct automatically. Yet, these misclassified pixels were easy to identify by hand by examining their spectra in ENVI.

Another problem was that the algorithm occasionally failed to classify the entire polymer particle, which led to a fragmentation of the particle in the classified image. As a result, the number of pixels had to be corrected manually using ENVI's Region of Interest Tool. It also occurred that pixels belonging to one plastic particle were classified as different polymer types. This had to be corrected by examining the spectra of every adjacent pixel of the classified particles.

In total, the necessary manual corrections were time-consuming and illustrate the need for further improvement of the automated PlaMAPP classification. However, this also applies to the Raman and FT-IR spectroscopy methods for which the spectra of classified particles also need to be checked by an expert to achieve reliable results for polymer identification and counting. Comparing only the measurement times of the three methods, NIR spectroscopy is about three orders of magnitude faster than FT-IR spectroscopy, which is in turn about three times faster than Raman spectroscopy (Table 1).

The main advantage of the near-infrared imaging spectroscopy presented here over other methods is the reduction in measurement time. If the reliability of the automated classification, which currently needs a mandatory detailed follow-up check, is further optimized, the PlaMAPP algorithm could contribute to significant time savings. Still, one limitation is the rather high MPP detection limit, which is about 100 µm, whereas FT-IR and Raman spectroscopy can detect even smaller microplastics, with a lower limit of 10–20 µm and 1–2 µm, respectively (Table 1).

Table 1 Comparison of measurement speeds of µ-Raman, FT-IR, and NIR spectroscopy. *The actual duration can vary according to the instrument settings used for spectral bandwidth, averaging methods and others. Individual information on measurement times can be found, e.g., in Löder et al. (2015), Primpke et al. (2020b), and Tagg et al. (2015)

	µ-Raman	FPA-based FT-IR	µ-NIR
Typical filter diameters	10 mm	11 mm	47 mm
Measurement times per filter	1 day*	10 h*	10 min
Measurement speed	0.055 mm^2/min	0.016 mm^2/min	173 mm^2/min
Lateral resolution, nominal	1 µm	20 µm	50 µm

3.2 MPP in Freshwater Samples

3.2.1 Surface Water Samples

In the detectable size fraction (> 100 µm), 222 MPPs were detected in the SFW samples. The mean MPP concentration was 0.65 MPP/L, with concentrations in individual samples ranging from 0.05 to 1.85 MPP/L (Fig. 3a). This is about an order of magnitude lower than water surface MPP concentrations of the Teltow Canal (tributary of the Havel River) (Schmidt et al., 2018), but is within the range of average concentrations of most European and North American rivers (Sarijan et al., 2021).

Yet, the measured concentration along the canal varies considerably along the canal and over time (May, June and July 2016) (Fig. 3). The highest range in MPP concentration along the canal within one sampling campaign was observed in May 2016 with 1.63 MPP/L whereby the lowest concentrations occurred at site SFW5 (0.2 MPP/L) and the highest at site SFW1 (1.85 MPP/L) (Fig. 3a). The average MPP concentration of all sampling points (SFW 1–SFW 5) dropped from 1.2 MPP/L in May 2016 to 0.37 MPP/L in June and July 2016. The reasons for the spatial and temporal variations have not been identified. However, possible explanations might include factors such as hydraulic disturbances caused by ship traffic and wind, although all samples were taken at the southern riverbank of the canal and each ship passage takes only about a few minutes. Unless determined otherwise, the spatial differences in observed MPP concentration might just reflect the natural variability of MPP occurrence in the uniformly constructed and shaped canal.

Three types of plastic polymers were identified in the canal (Fig. 4). The majority of MPP are PP (50.4% on average for all sample dates) and PE (48.2%), and

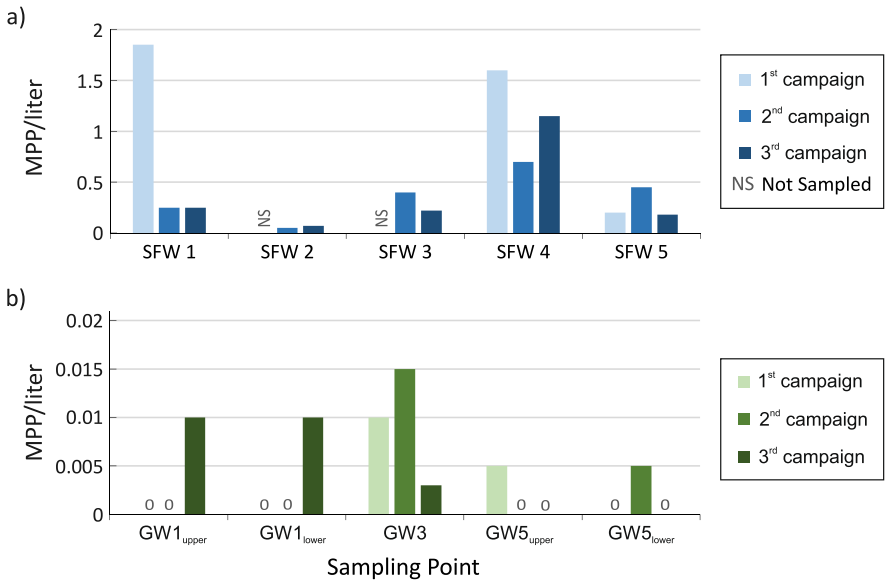

Fig. 3 Microplastic particle abundances in (**a**) the Lower Havel river (MPP > 100 µm) and (**b**) adjacent groundwater (100 < MPP < 2000 µm) of the three sampling campaigns carried out

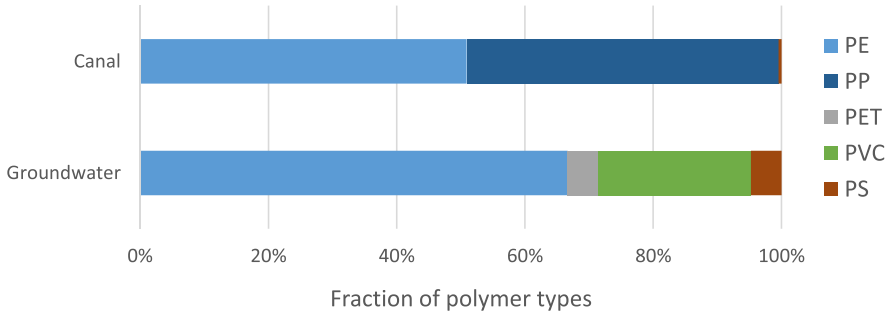

Fig. 4 Polymer types in the surface water samples (in total 222 particles detected) and groundwater (in total 21 particles detected)

these polymer types were found in all samples (except two samples that only comprised PP; SFW2, and SFW4, 2nd campaign). This matches the expectation that predominantly lower-density MPP accumulate in the topmost part of the water column (which can lead to overestimations of total MPP loads) and is in accordance with previous findings, showing that PE and PP were dominant in other freshwater resources (e.g. Fiore et al., 2022; Mani et al., 2016; Schmidt et al., 2018). Even the regular ship traffic and the subsequent turbulent mixing of the entire canal did not affect such a distinct stratification of MPP. Additionally, one PS was found in SFW3 (3rd campaign). No spatial or temporal trend was discernible with respect to polymer type proportions, neither among sampling locations nor among the campaigns.

3.2.2 Groundwater Samples

A substantial number of blue PVC particles were found in the GW samples (> 70% of all MPP), which could be clearly assigned to the well casings. We excluded these particles from the results to enable the interpretation with regard to the groundwater MPP load independent of these identified cross-contaminants. While the source of the blue PVC particles could be clearly determined, this was not the case for the rest of the MPP found in the GW samples, since none of the sampling equipment matched the remaining MPP with respect to their colour and polymer type.

In total, 21 MPP were found in all groundwater samples. The mean MPP concentration was 0.004 MPP/L. The concentrations in individual samples ranged from 0 to 0.015 MPP/L (Fig. 3b). Thus, MPP concentrations in groundwater were about two orders of magnitude lower than in the adjacent surface water, but comparable to concentrations detected in drinking water from groundwater sources (Mintenig et al., 2019). In eight out of our 15 samples analysed, no MPP were detected (Fig. 3b). However, Johnson et al. (2020) found average MPP concentrations of 2.3 MPP/L in raw water of three water treatment works that directly abstract bank filtrate from chalk and sandstone aquifers. In their study, microplastics were not consistently present in the raw water at five separate sampling occasions over the period between August 2018 and May 2019. And in 10 out of 15 analysed raw water samples, no MPP were detected (Johnson et al., 2020).

These results indicate that MPP might be partly filtered out during bank filtration within the aquifer, though not always completely, but this tendency may also be caused by temporal variations in the input concentrations from the canal that were not captured by the temporal resolution (duration and frequency) of our sampling campaigns. In contrast, seven samples show slight MPP loads (Fig. 3b). Considering only the samples with quantifiable MPP, then on average, 0.01 MPP/L was present in the groundwater. Overall about 98.5% of all microplastic particles above 100 µm were filtered out during bank filtration passage through the medium- to coarse-grained sandy aquifer. Nonetheless, these findings suggest a potential risk of MPP leaching into groundwater through bank filtration requiring further investigation on MPP transport in sand and gravel aquifers towards pumping wells of water works to see if this could cause a pollution of drinking water supplies.

Four types of polymers were identified in the pumped GW samples: PE, PVC, PET, and PS. The most abundant type of polymer is PE at 67% ($n_{PE} = 14$) followed by PVC at 24% ($n_{PVC} = 5$) (Fig. 4). Only one trace of PET and PS each was found in the groundwater samples. Observed types of polymers in the pumped GW samples substantially varied in space, yet without clear patterns or trends. Conspicuously, PVC was only found in the well with the shortest residence time between the canal and the observation well (flow velocity ~ 0.4 m/d). In contrast to the SFW, no PP particles were found in the GW samples. However, not finding PP particles in the GW samples might be just a result of the low particle density, which would prevent PP particles from descending into the SFW and infiltrating into the GW.

The particle sizes ranged from 0.005 to 0.62 mm^2. The number of MPP exponentially decreased with increasing particle size (Fig. 5). The minimum diameter of detected MPP ranged from 100.0 to 700.0 µm, and 87% of the particles had a minimum particle diameter ≤ 300 µm (Fig. 5). Two particles had markedly larger minimum diameters of 700 µm (PE in $GW1_{upper}$, 3rd campaign) and 425 µm (PE in $GW3_{upper}$, 1st campaign). All other particles were much smaller, ranging from 100 to 300 µm in diameter (mean = 200 µm).

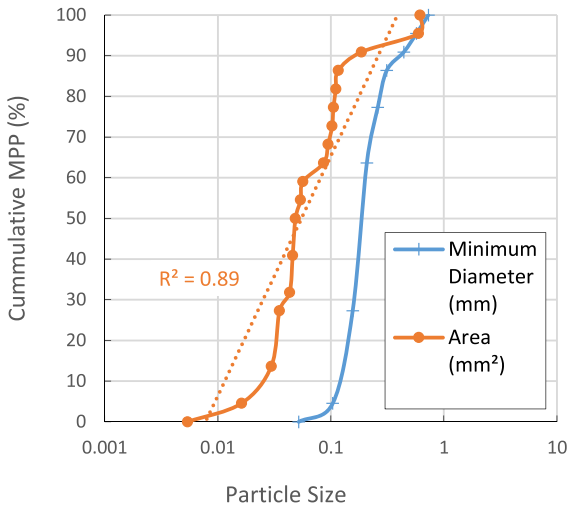

Fig. 5 Cumulative distribution of MPP particle sizes (Minimum Particle Diameter and Area) in the groundwater samples, with fitted logarithmic function to MPP Area (dotted line, goodness of fit is shown as R^2)

In view of the medium- to coarse-grained sand that is predominant in our study area, particles of up to 308 µm in size could potentially enter the aquifer (Herzig et al., 1970; Frey et al., 1999). This corresponds well to the mean diameters detected in our observations, as well as to MPP dimensions recently found in streambed sediments (Frei et al., 2019), drinking water production wells (Mintenig et al., 2019; Johnson et al., 2020), and tap water (Kirstein et al., 2021). The occurrence of some larger particles might be related to local heterogeneities in the coarse-grained sediment, and the relatively high subsurface flow velocities at the study site in comparison to other lowland groundwater situations.

Just as in this study, most GW observation wells that are in operation are very likely substantially polluted with MPP due to regular measurements with sampling equipment made of common plastic (e.g. electric contact meters). For example, Samandra et al. (2022) reported substantial microplastic pollution in a GW borehole of an alluvial, unconfined aquifer in Australia (38 MPP/L on average), which is several orders of magnitude higher compared to our results. However, they took 1 L groundwater samples with a stainless-steel bailer attached to a braided polyamide rope from the borehole without purging the bores prior to sampling. Our own comparison showed that bailed (prior to pumping with a stainless-steel bailer attached to a braided hemp rope) MPP concentrations were about three orders of magnitude higher (1.35 MPP/L) than pumped MPP and also clearly above mean SFW MPP concentrations. Therefore, we argue that observation boreholes need to be purged prior to sampling to remove artificial MPP accumulation and sample recharging GW only. Beyond that, our results indicate that extensive research is required to gain a better understanding of the occurrence, fate, and transport of microplastics in groundwater systems. This also includes a detailed monitoring of the potential input concentration from the SFW to capture seasonal trends and variations. To minimize the risk of sampling contaminated well water, we recommend discarding several hundreds of liters of water prior to sampling. With respect to the overall low MPP concentrations in groundwater, the sampling volumes should be further increased to several hundreds of liters (as in this study and Johnson et al., 2020) in order to achieve representative values for the presence of MPP.

3.3 MPP in Beach Sediment Samples

3.3.1 Beach Transect Heiligensee and Hüttelmoor

In total, 21 MPP were found at the beach transect Heiligensee and Hüttelmoor and the number of detected particles per sample varied from one to four. Average MPP concentrations of all three samples over all depths were 6.3 MPP/kg at the beach, 4.3 MPP/kg on the dune, and 4.4 MPP/kg at the rear site of the dune (Fig. 6a). The average MPP abundance per depth increased from 3.7 MPP/kg at 5 cm depth to 7.8 MPP/kg at 40 cm. This corresponds to a 2.2-fold increase over the entire profile (Fig. 6a), albeit with a large variance at each depth.

Of the particles found, 71% were classified as PE, 19% as PP, and 10% as PS (Fig. 7). The particle sizes ranged from 0.005 to 0.806 mm^2. The number of MPP exponentially decreased with increasing particle size (Fig. 8). We identified major differences in particle dimensions per MPP type. While the identified PE particles cover all size ranges, the PP particles vary in size from 0.011 to 0.068 mm^2 and the two PS particles measure 0.022 mm^2 and 0.032 mm^2, only.

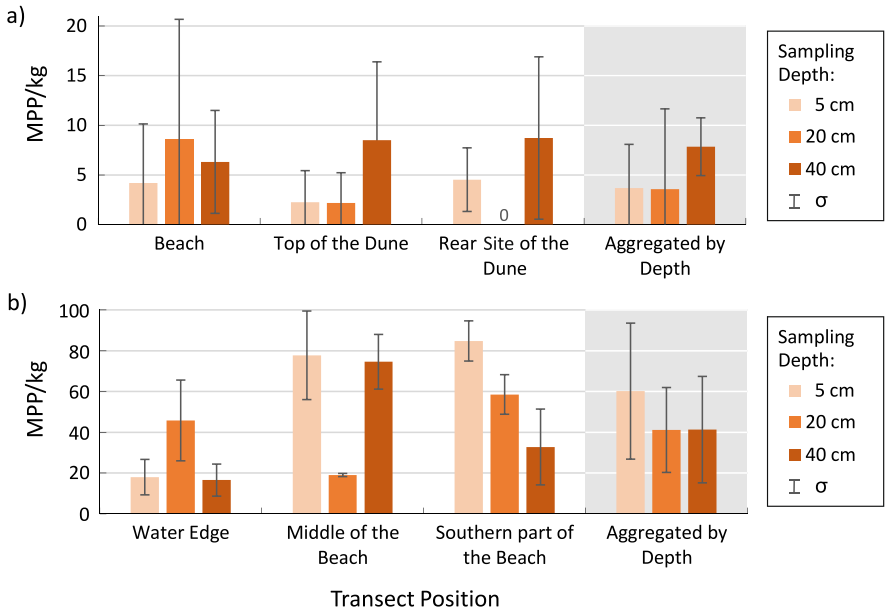

Fig. 6 Microplastic particle abundances (per kg dry weight) at the beaches in (**a**) Heiligensee and Hüttelmoor and (**b**) Warnemünde for each position along the transects and sampling depths (average of three individual samples, the standard deviation of all samples is shown by the black lines), as well as MPP abundances aggregated by depth (100 < MPP < 2000 µm)

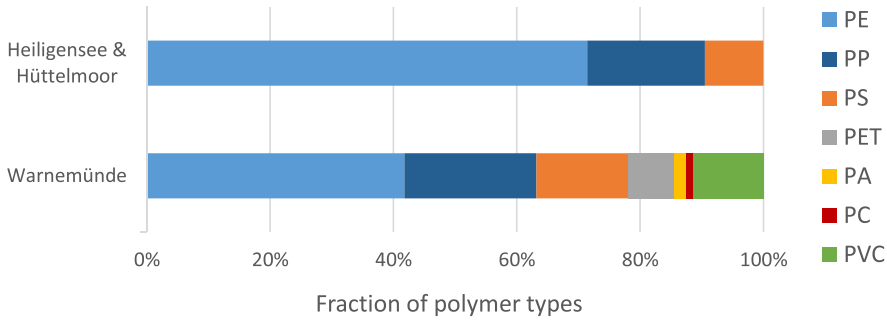

Fig. 7 Polymer types in the beach sediments of Heiligensee and Hüttelmoor (in total 21 particles detected) and Warnemünde (in total 201 particles detected)

3.3.2 Beach Transect Warnemünde

In total, 201 MPP were identified at the beach transect Warnemünde. The number of detected particles per sample varied from eight to 16 MPP (Fig. 6b). Depth-average MPP concentrations ranged between 26.9 MPP/kg at the water's edge, 56.8 MPP/kg in the middle of the beach, and 58.7 MPP/kg on the southern part of the beach. MPP abundances significantly increased between the water's edge and the two beach locations (p-value = 0.03, Fig. 6b). Average MPP abundances per depth decreased from 60.2 MPP/kg at 5 cm to about 41 MPP/kg at 20 cm and 40 cm (Fig. 6b) and thus decreased by a factor of 0.7, but again, with a large variance at each depth.

The applied density separation method using high-density NaI solution is suitable for separating even highly dense pristine polymer materials such as PVC, PET, and PA (according to common literature values, their densities range from 1.2 to 1.7 g/cm^3) from the matrix components. Of the confirmed MPPs, PE particles were dominant at 41.4%, while 21.2% were classified as PP, 14.8% as PS, 11.3% as PVC, 7.4% as PET, 2% as PA, and about 1% as PC (Fig. 7). The beach stretch of Warnemünde showed a very wide variety of particle sizes ranging from 0.005 up to 44.94 mm^2. The number of MPP exponentially decreased with increasing particle size (Fig. 8).

3.3.3 Comparison Between the Two Beach Study Sites

The range of detected MPP concentrations at both sites is comparable to values found along beaches of the Baltic Sea (Dekiff et al., 2014; Graca et al., 2017). The study area in Warnemünde contains a

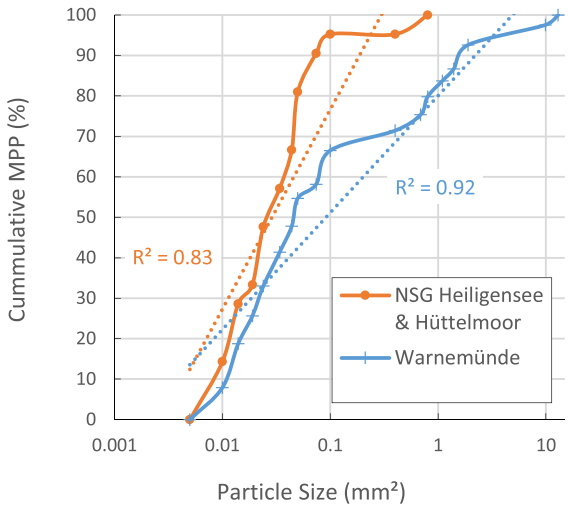

Fig. 8 Cumulative distribution of MPP particle size in the beach samples of Heiligensee and Hüttelmoor and Warnemünde, with fitted logarithmic function (dotted lines, quality of fit is shown as R^2)

significantly higher MPP load (47.5 ± 5.6 MPP/kg) compared to the beach at Heiligensee and Hüttelmoor (5.0 ± 1.4 MPP/kg) (p-value $= 3.3 \times 10^{-9}$). This underpins the findings of Browne et al. (2011), who found a correlation between MPP abundance and the anthropogenic population density on shorelines worldwide. However, recent studies demonstrate that this is not always the case, as MPP abundances in national parks and urban beaches do not necessarily differ substantially (Esiukova, 2017; Urban-Malinga et al., 2020).

While several polymer types were identified in the Warnemünde samples that did not occur at Heiligensee and Hüttelmoor, PE was clearly dominant at both sites, followed by PP and PS particles. The dominance of these three polymer types is a common finding in studies of beach sediments worldwide (e.g. Imhof et al., 2012; Sathish et al., 2019; Wessel et al., 2016). At both locations, MPP abundances increased with decreasing particle size, which is consistent with results from other surveys (e.g. Claessens et al., 2011; Graca et al., 2017). Spectroscopic analyses of microplastic particles (ranging from 10 µm to 2 mm) of sediment samples taken at comparable beach locations in 2021 confirmed this trend and additionally highlighted that the abundance of MPP ranging from 10 to 100 µm was more than two (Heiligensee and Hüttelmoor) to three (Warnemünde) times higher compared to MPP ranging from 100 µm to 2 mm (Heidrich, 2022). For small particles (≤ 0.07 mm^2), the MPP size distributions of the two locations are very similar, but they differ substantially for larger particles (Fig. 8). This is partly because all MPP at Heiligensee and Hüttelmoor were smaller than 1~mm^2, while 16% of MPP at Warnemünde exceeded 1~mm^2. This might be related to the different origins of the particles at the two beach transects. At the touristic beach in Warnemünde, the risk of direct MPP input due to intense human activities is high. This also matches the finding that the sampling location in the middle of the beach is the most polluted part within the transect, compared to e.g. the water's edge.

4 Conclusions

Overall, the application of near-infrared imaging spectroscopy with the subsequent data analysis using the PlaMAPP routine is suitable to quantitatively analyse high numbers of environmental samples in order to detect microplastic particles larger than 100~µm in a reliable, and non-destructive way. Nevertheless, there are still some issues known from previous studies with lower resolution regarding the correct classification of MPP. This is mainly due to the lack of difference between PE particles and organic materials that requires a detailed follow-up correction based on the visual inspection of the recorded spectra.

The data achieved in terms of microplastic concentrations constitute a solid estimate of the MPP abundance in freshwaters and sediments. In the beach samples, we found lower MPP concentrations at the natural reserve Heiligensee and Hüttelmoor (5.5~MPP/kg) than at the highly frequented Warnemünde beach (47.5~MPP/kg). The mean river MPP concentration of 0.65~MPP/L and the dominance of PE and PP in the topmost part of the water column were comparable to other rivers. The adjacent groundwater concentrations were about two orders of magnitude lower (0.004~MPP/L). The majority of particles in the GW samples were < 300~µm, which indicates the upper size limit of possibly mobile MPP within the medium- to coarse-grained sandy aquifer. These findings suggest a potential risk of MPP leaching into groundwater via bank filtration and thus highlight the need for more detailed research on the occurrence, fate, and transport of microplastics in groundwater systems.

Acknowledgements To merge the necessarily recorded three strips of one filter into a single image, an in-house Python-based software written by Daniel Scheffler from GFZ Potsdam was used. We thank Daniel for an introduction to the use of his software AROSICS and for helping to adapt it to the mosaicking of lab-recorded images.

Author Contribution SO and MM conceived the study. LK and JK executed the study of the water and beach samples, respectively. LKS supported freshwater sampling. MBo mainly developed and adapted the PLAMAPP algorithm and provided guidance in the process of NIR processing and MPP detection. MBe and CGB introduced JK to the process of density separation and provided lab equipment. MBo, MM, and SO worked on summarizing the PlaMAPP algorithms. All authors contributed to the development and writing of the manuscript.

Funding Open Access funding enabled and organized by Projekt DEAL.

Data Availability All data that support the findings of this study are included in the article, as well as any supplementary files.

Declarations

Ethics Approval and Consent to Participate Not applicable

Consent for Publication Not applicable.

Competing Interests The authors declare no competing interests.

References

Atwood, E. C., Falcieri, F. M., Piehl, S., Bochow, M., Matthies, M., Franke, J., Carniel, S., Sclavo, M., Laforsch, C., & Siegert, F. (2019). Coastal accumulation of microplastic particles emitted from the Po River, Northern Italy: Comparing remote sensing and hydrodynamic modelling with in situ sample collections. *Marine Pollution Bulletin, 138*, 561–574. https://doi.org/10.1016/j.marpolbul.2018.11.045

Barroso, Á., Kemper, B., Ketelhut, S., Graß, S., Reiber, J., Schnekenburger, J., (2019). Multimodal optical detection and toxicity testing of microplastics in the environment. Proc. SPIE 10881, Imaging, Manipulation, and Analysis of Biomolecules, Cells, and Tissues XVII, 108811C (4 March 2019); https://doi.org/10.1117/12.2510737

Bednarz, M., Obermaier, N., Bannick, C.G., (2020). Density separation of soils as sample preparation for the determination of plastics, in: EGU General Assembly 2020, Online, 4–8 May 2020, EGU2020-22555. https://doi.org/10.5194/egusphere-egu2020-22555

Boos, J.-P., Gilfedder, B. S., & Frei, S. (2021). Tracking microplastics across the streambed interface: Using laser-induced-fluorescence to quantitatively analyze microplastic transport in an experimental flume. *Water Resources Research, 57*, e2021WR031064. https://doi.org/10.1029/2021WR031064

Braun, Ulrike, Altmann, K., Bannick, C. G., Becker, R., Bitter, H., Bochow, M., Dierkes, G., Enders, K., et al. (2021). Analysis of microplastics - Sampling, preparation and detection methods. Status report within the framework program plastics in the environment. https://bmbf-plastik.de/sites/default/files/2021-12/Status%20Report_Analysis%20%20Microplastics_PidU_May_2021_0.pdf

Browne, M. A., Crump, P., Niven, S. J., Teuten, E., Tonkin, A., Galloway, T., & Thompson, R. (2011). Accumulation of microplastic on shorelines worldwide: Sources and sinks. *Environmental Science and Technology, 45*, 9175–9179. https://doi.org/10.1021/es201811s

Claessens, M., Meester, S. D., Landuyt, L. V., Clerck, K. D., & Janssen, C. R. (2011). Occurrence and distribution of microplastics in marine sediments along the Belgian coast. *Marine Pollution Bulletin, 62*, 2199–2204. https://doi.org/10.1016/j.marpolbul.2011.06.030

Dekiff, J. H., Remy, D., Klasmeier, J., & Fries, E. (2014). Occurrence and spatial distribution of microplastics in sediments from Norderney. *Environmental Pollution, 186*, 248–256. https://doi.org/10.1016/j.envpol.2013.11.019

Drummond, J. D., Nel, H. A., Packman, A. I., & Krause, S. (2020). Significance of hyporheic exchange for predicting microplastic fate in rivers. *Environmental Science & Technology Letters, 7*, 727–732. https://doi.org/10.1021/acs.estlett.0c00595

Eerkes-Medrano, D., Thompson, R. C., & Aldridge, D. C. (2015). Microplastics in freshwater systems: A review of the emerging threats, identification of knowledge gaps and prioritisation of research needs. *Water Research, 75*, 63–82. https://doi.org/10.1016/j.watres.2015.02.012

Esiukova, E. (2017). Plastic pollution on the Baltic beaches of Kaliningrad region, Russia. *Marine Pollution Bulletin, 114*, 1072–1080. https://doi.org/10.1016/j.marpolbul.2016.10.001

Esiukova, E., Lobchuk, O., Haseler, M., & Chubarenko, I. (2021). Microplastic contamination of sandy beaches of national parks, protected and recreational areas in southern parts of the Baltic Sea. *Marine Pollution Bulletin, 173*, 113002. https://doi.org/10.1016/j.marpolbul.2021.113002

Faltynkova, A., Johnsen, G., & Wagner, M. (2021). Hyperspectral imaging as an emerging tool to analyze microplastics: A systematic review and recommendations for future development. *Microplastics and Nanoplastics, 1*, 13. https://doi.org/10.1186/s43591-021-00014-y

Fiore, L., Serranti, S., Mazziotti, C., Riccardi, E., Benzi, M., & Bonifazi, G. (2022). Classification and distribution of freshwater microplastics along the Italian Po river by hyperspectral imaging. *Environmental Science and Pollution Research, 29*, 48588–48606. https://doi.org/10.1007/s11356-022-18501-x

Frei, S., Piehl, S., Gilfedder, B. S., Löder, M. G. J., Krutzke, J., Wilhelm, L., & Laforsch, C. (2019). Occurence of microplastics in the hyporheic zone of rivers. *Science and Reports, 9*, 15256. https://doi.org/10.1038/s41598-019-51741-5

Frey, J. M., Schmitz, P., Dufreche, J., & Pinheiro, I. G. (1999). Particle Deposition in Porous Media: Analysis of Hydrodynamic and Weak Inertial Effects. *Transport in Porous Media, 37*, 25–54. https://doi.org/10.1023/A:1006546717409

Goeppert, N., & Goldscheider, N. (2021). Experimental field evidence for transport of microplastic tracers over large distances in an alluvial aquifer. *J Hazard Mater, 408*, 124844. https://doi.org/10.1016/j.jhazmat.2020.124844

Graca, B., Szewc, K., Zakrzewska, D., Dołęga, A., & Szczerbowska-Boruchowska, M. (2017). Sources and fate of microplastics in marine and beach sediments of the Southern Baltic Sea—A preliminary study. *Environmental Science and Pollution Research, 24*, 7650–7661. https://doi.org/10.1007/s11356-017-8419-5

Harris, P. T. (2020). The fate of microplastic in marine sedimentary environments: A review and synthesis. *Marine Pollution Bulletin, 158*, 111398. https://doi.org/10.1016/j.marpolbul.2020.111398

Heidrich, Y. (2022). *Raman-spektroskopische Analyse von Mikroplastikpartikeln aus Strandsedimenten von der Nord- und Ostseeküste*. University of Potsdam.

Herzig, J., Leclerc, D., & Goff, P. L. (1970). Flow of suspensions through porous media—application to deep filtration. *Industrial & Engineering Chemistry Research, 62*, 8–35. https://doi.org/10.1021/ie50725a003

Hidalgo-Ruz, V., Gutow, L., Thompson, R. C., & Thiel, M. (2012). Microplastics in the marine environment: A review of the methods used for identification and quantification. *Environmental Science and Technology, 46*, 3060–3075. https://doi.org/10.1021/es2031505

Imhof, H. K., Schmid, J., Niessner, R., Ivleva, N. P., & Laforsch, C. (2012). A novel, highly efficient method for the separation and quantification of plastic particles in sediments of aquatic environments: Novel plastic particle separation method. *Limnology and Oceanography: Methods, 10*, 524–537. https://doi.org/10.4319/lom.2012.10.524

Ivleva, N. P. (2021). Chemical analysis of microplastics and nanoplastics: Challenges, advanced methods, and perspectives. *Chemical Reviews, 121*, 11886–11936. https://doi.org/10.1021/acs.chemrev.1c00178

Jeszenszky, É., Kocsányi, L., & Richter, P. (2004). Eliminating the interference pattern in near-infrared spectra used for identification of thin plastic foils. *Applied Spectroscopy, 58*, 693–697. https://doi.org/10.1366/000370204872953

Johnson, A. C., Ball, H., Cross, R., Horton, A. A., Jürgens, M. D., Read, D. S., Vollertsen, J., & Svendsen, C. (2020). Identification and quantification of microplastics in potable water and their sources within water treatment works in England and Wales. *Environmental Science and Technology, 54*, 12326–12334. https://doi.org/10.1021/acs.est.0c03211

Jurasinski, G., Janssen, M., Voss, M., Böttcher, M. E., Brede, M., Burchard, H., Forster, S., Gosch, L., Gräwe, U., Gründling-Pfaff, S., Haider, F., Ibenthal, M., Karow, N., Karsten, U., Kreuzburg, M., Lange, X., Leinweber, P., Massmann, G., Ptak, T., … Lennartz, B. (2018). Understanding the coastal ecocline: Assessing sea–land interactions at non-tidal, low-lying coasts through interdisciplinary research. *Frontiers in Marine Science, 5*, 342. https://doi.org/10.3389/fmars.2018.00342

Kirstein, I. V., Hensel, F., Gomiero, A., Iordachescu, L., Vianello, A., Wittgren, H. B., & Vollertsen, J. (2021). Drinking plastics? – Quantification and qualification of microplastics in drinking water distribution systems by µFTIR and Py-GCMS. *Water Research, 188*, 116519. https://doi.org/10.1016/j.watres.2020.116519

Koelmans, A. A., Mohamed Nor, N. H., Hermsen, E., Kooi, M., Mintenig, S. M., & De France, J. (2019). Microplastics in freshwaters and drinking water: Critical review and assessment of data quality. *Water Research, 155*, 410–422. https://doi.org/10.1016/j.watres.2019.02.054

Kumar, R., Sharma, P., Manna, C., & Jain, M. (2021). Abundance, interaction, ingestion, ecological concerns, and mitigation policies of microplastic pollution in riverine ecosystem: A review. *Science of The Total Environment, 782*, 146695. https://doi.org/10.1016/j.scitotenv.2021.146695

Li, J., Liu, H., & Paul Chen, J. (2018). Microplastics in freshwater systems: A review on occurrence, environmental effects, and methods for microplastics detection. *Water Research, 137*, 362–374. https://doi.org/10.1016/j.watres.2017.12.056

Löder, M. G. J., & Gerdts, G. (2015). Methodology used for the detection and identification of microplastics—A critical appraisal. In M. Bergmann, L. Gutow, & M. Klages (Eds.), *Marine anthropogenic litter* (pp. 201–227). Cham: Springer International Publishing. https://doi.org/10.1007/978-3-319-16510-3_8

Löder, M. G. J., Kuczera, M., Mintenig, S., Lorenz, C., & Gerdts, G. (2015). Focal plane array detector-based micro-Fourier-transform infrared imaging for the analysis of microplastics in environmental samples. *Environmental Chemistry, 12*, 563–581.

Mani, T., Hauk, A., Walter, U., & Burkhardt-Holm, P. (2016). Microplastics profile along the Rhine River. *Science and Reports, 5*, 17988. https://doi.org/10.1038/srep17988

Miegel, K., Gräff, T., Franck, C., Salzmann, T., Bronstert, A., Walther, M., Oswald, S. E. (2017). *Auswirkungen des Sturmhochwassers der Ostsee am 4./5. Januar 2017 auf das renaturierte Niedermoor„ Hütelmoor und Heiligensee" an der deutschen Ostseeküste*. Hydrologie und Wasserbewirtschaftung / BfG – Jahrgang: 61.2017 4. https://doi.org/10.5675/HYWA_2017,4_2

Mielke, C., Boesche, N. K., Rogass, C., Kaufmann, H., & Gauert, C. (2015). New geometric hull continuum removal algorithm for automatic absorption band detection from spectroscopic data. *Remote Sensing Letters, 6*, 97–105. https://doi.org/10.1080/2150704X.2015.1007246

Mintenig, S. M., Löder, M. G. J., Primpke, S., & Gerdts, G. (2019). Low numbers of microplastics detected in drinking water from ground water sources. *Science of the Total Environment, 648*, 631–635. https://doi.org/10.1016/j.scitotenv.2018.08.178

Munz, M., Oswald, S. E., & Schmidt, C. (2017). Coupled long-term simulation of reach-scale water and heat fluxes

across the river-groundwater interface for retrieving hyporheic residence times and temperature dynamics. *Water Resources Research, 53*, 8900–8924. https://doi.org/10.1002/2017WR020667

Munz, M., Oswald, S. E., Schäfferling, R., & Lensing, H.-J. (2019). Temperature-dependent redox zonation, nitrate removal and attenuation of organic micropollutants during bank filtration. *Water Research, 162*, 225–235. https://doi.org/10.1016/j.watres.2019.06.041

Nizzetto, L., Bussi, G., Futter, M. N., Butterfield, D., & Whitehead, P. G. (2016). A theoretical assessment of microplastic transport in river catchments and their retention by soils and river sediments. *Environmental Science. Processes & Impacts, 18*, 1050–1059. https://doi.org/10.1039/c6em00206d

Panno, S. V., Kelly, W. R., Scott, J., Zheng, W., McNeish, R. E., Holm, N., Hoellein, T. J., & Baranski, E. L. (2019). Microplastic contamination in Karst groundwater systems. *Groundwater, 57*, 189–196. https://doi.org/10.1111/gwat.12862

Piehl, S., Atwood, E.C., Bochow, M., Imhof, H.K., Franke, J., Siegert, F., Laforsch, C. (2020). Can water constituents be used as proxy to map microplastic dispersal within transitional and coastal waters? Front Environ Sci 8:92. https://doi.org/10.3389/fenvs.2020.00092

Pittroff, M., Müller, Y. K., Witzig, C. S., Scheurer, M., Storck, F. R., & Zumbülte, N. (2021). Microplastic analysis in drinking water based on fractionated filtration sampling and Raman microspectroscopy. *Environmental Science and Pollution Research, 28*, 59439–59451. https://doi.org/10.1007/s11356-021-12467-y

Primpke, S., Christiansen, S. H., Cowger, W., De Frond, H., Deshpande, A., Fischer, M., Holland, E. B., Meyns, M., O'Donnell, B. A., Ossmann, B. E., Pittroff, M., Sarau, G., Scholz-Böttcher, B. M., & Wiggin, K. J. (2020a). Critical assessment of analytical methods for the harmonized and cost-efficient analysis of microplastics. *Applied Spectroscopy, 74*, 1012–1047. https://doi.org/10.1177/0003702820921465

Primpke, S., Godejohann, M., & Gerdts, G. (2020b). Rapid identification and quantification of microplastics in the environment by quantum cascade laser-based hyperspectral infrared chemical imaging. *Environmental Science and Technology, 54*, 15893–15903. https://doi.org/10.1021/acs.est.0c05722

Quinn, B., Murphy, F., & Ewins, C. (2017). Validation of density separation for the rapid recovery of microplastics from sediment. *Analytical Methods, 9*, 1491–1498. https://doi.org/10.1039/C6AY02542K

R Core Team. (2021). R: A language and environment for statistical computing. R Foundation for Statistical Computing, Vienna, Austria.

Sagawa, N., Kawaai, K., & Hinata, H. (2018). Abundance and size of microplastics in a coastal sea: Comparison among bottom sediment, beach sediment, and surface water. *Marine Pollution Bulletin, 133*, 532–542. https://doi.org/10.1016/j.marpolbul.2018.05.036

Samandra, S., Johnston, J. M., Jaeger, J. E., Symons, B., Xie, S., Currell, M., Ellis, A. V., & Clarke, B. O. (2022). Microplastic contamination of an unconfined groundwater aquifer in Victoria, Australia. *Science of The Total Environment, 802*, 149727. https://doi.org/10.1016/j.scitotenv.2021.149727

Sarijan, S., Azman, S., Said, M. I. M., & Jamal, M. H. (2021). Microplastics in freshwater ecosystems: A recent review of occurrence, analysis, potential impacts, and research needs. *Environmental Science and Pollution Research, 28*, 1341–1356. https://doi.org/10.1007/s11356-020-11171-7

Sathish, N., Jeyasanta, K. I., & Patterson, J. (2019). Abundance, characteristics and surface degradation features of microplastics in beach sediments of five coastal areas in Tamil Nadu, India. *Marine Pollution Bulletin, 142*, 112–118. https://doi.org/10.1016/j.marpolbul.2019.03.037

Scheffler, D. AROSICS: An automated and robust open-source image co-registration software for multi-sensor satellite data, *Zenodo*, https://doi.org/https://zenodo.org/record/4601166 (2021).

Scheffler, D., Hollstein, A., Diedrich, H., Segl, K., & Hostert, P. (2017). AROSICS: An automated and robust open-source image co-registration software for multi-sensor satellite data. *Remote Sensing, 9*, 676. https://doi.org/10.3390/rs9070676

Schmidt, L. K., Bochow, M., Imhof, H. K., & Oswald, S. E. (2018). Multi-temporal surveys for microplastic particles enabled by a novel and fast application of SWIR imaging spectroscopy – Study of an urban watercourse traversing the city of Berlin, Germany. *Environmental Pollution, 239*, 579–589. https://doi.org/10.1016/j.envpol.2018.03.097

Schreiber, L., Munz, M., Salzmann, T., & Oswald, S. E. (2021). Modellierung der Strömungsdynamik in einem revitalisierten Küstenmoorgebiet an der Ostsee. *Grundwasser, 26*, 289–304. https://doi.org/10.1007/s00767-021-00486-y

Schröder, K., Kossel, E., & Lenz, M. (2021). Microplastic abundance in beach sediments of the Kiel Fjord, Western Baltic Sea. *Environmental Science and Pollution Research, 28*, 26515–26528. https://doi.org/10.1007/s11356-020-12220-x

Stolte, A., Forster, S., Gerdts, G., & Schubert, H. (2015). Microplastic concentrations in beach sediments along the German Baltic coast. *Marine Pollution Bulletin, 99*, 216–229. https://doi.org/10.1016/j.marpolbul.2015.07.022

Tagg, A. S., Sapp, M., Harrison, J. P., & Ojeda, J. J. (2015). Identification and quantification of microplastics in wastewater using focal plane array-based reflectance micro-FT-IR imaging. *Analytical Chemistry, 87*, 6032–6040. https://doi.org/10.1021/acs.analchem.5b00495

Tötzke, C., Oswald, S. E., Hilger, A., & Kardjilov, N. (2021). Non-invasive detection and localization of microplastic particles in a sandy sediment by complementary neutron and X-ray tomography. *Journal of Soils and Sediments, 21*, 1476–1487. https://doi.org/10.1007/s11368-021-02882-6

Urban-Malinga, B., Zalewski, M., Jakubowska, A., Wodzinowski, T., Malinga, M., Pałys, B., & Dąbrowska, A. (2020). Microplastics on sandy beaches of the southern Baltic Sea. *Marine Pollution Bulletin, 155*, 111170. https://doi.org/10.1016/j.marpolbul.2020.111170

Viaroli, S., Lancia, M., & Re, V. (2022). Microplastics contamination of groundwater: Current evidence and future perspectives. A review. *Sci Total Environ, 824*, 153851. https://doi.org/10.1016/j.scitotenv.2022.153851

Waldschläger, K., & Schüttrumpf, H. (2020). Infiltration behavior of microplastic particles with different densities, sizes, and shapes—From glass spheres to natural

sediments. *Environmental Science and Technology, 54*, 9366–9373. https://doi.org/10.1021/acs.est.0c01722

Wang, W., & Wang, J. (2018). Investigation of microplastics in aquatic environments: An overview of the methods used, from field sampling to laboratory analysis. *TrAC Trends in Analytical Chemistry, 108*, 195–202. https://doi.org/10.1016/j.trac.2018.08.026

Weisser, J., Pohl, T., Heinzinger, M., Ivleva, N. P., Hofmann, T., & Glas, K. (2022). The identification of microplastics based on vibrational spectroscopy data – A critical review of data analysis routines. *TrAC Trends in Analytical Chemistry, 148*, 116535. https://doi.org/10.1016/j.trac.2022.116535

Wessel, C. C., Lockridge, G. R., Battiste, D., & Cebrian, J. (2016). Abundance and characteristics of microplastics in beach sediments: Insights into microplastic accumulation in northern Gulf of Mexico estuaries. *Marine Pollution Bulletin, 109*, 178–183. https://doi.org/10.1016/j.marpolbul.2016.06.002